Materials Advances

ROYAL SOCIETY OF CHEMISTRY

PAPER

View Article Online
View Journal

Cite this: DOI: 10.1039/d6ma00335d

Extra-low resistivity in N and H doped Cu_2O thin films grown by room temperature RF sputtering

A. Di Trolio, *[a] P. M. Latino,[a] B. Paci,[a] A. Generosi,[a] A. Cricenti,[a] M. Luce,[a] D. Becerrill,[a] A. Di Carlo,[ab] S. Alì,[ab] F. Filippone[c] and A. Amore Bonapasta[c]

Received 10th March 2026,
Accepted 11th May 2026

DOI: 10.1039/d6ma00335d

rsc.li/materials-advances

Cuprous oxide (Cu_2O) is an intrinsic p-type semiconductor representing an interesting, potential hole transporting material in 3rd generation solar cells. However, its practical applications are significantly limited by its intrinsically high resistivity. In the present study, we show that polycrystalline Cu_2O thin films with an extra-low resistivity of 0.16 Ω cm can be grown by radio frequency (RF) sputtering by exploiting the effects of nitrogen and hydrogen doping. Significantly and differently from previous studies, the films are deposited at room temperature and the material doping is performed through the simultaneous introduction of both dopants in the Cu_2O films during the growth process. The effects of N and H dopants on the Cu_2O properties are investigated by performing resistivity, Hall effect, UPS, X-ray Diffraction and Raman measurements on a pristine Cu_2O film, on Cu_2O films doped with N and H individually, as well as on films containing both dopants. Such a systematic investigation of the doping effects permits to perform a comparative analysis of the achieved results and data from literature and to develop an exhaustive, interpretative framework that clarifies the role of native defects and N and H dopants in reducing the resistivity of Cu_2O.

1. Introduction

Cuprous oxide, Cu_2O, is a spontaneous p-type semiconductor characterized by a direct bandgap in the range of 1.9 eV and 2.6 eV, and a high absorption coefficient of 10^6 cm^{-1}.[1] Owing to its non-toxic nature and low production cost, Cu_2O has attracted considerable interest for applications in optoelectronic devices. Over the past decades, extensive research has focused on the use of Cu_2O as an absorption layer in thin-film solar cells, as the theoretical power conversion efficiency (PCE) of Cu_2O-based solar cells has been estimated to approach 20%.[1,2] However, despite this promising theoretical potential, the highest energy conversion efficiency of Cu_2O based solar cells reported so far is still below 10%.[3–5] With the advent of perovskite materials for the 3rd generation solar cells, whose efficiency surpassed the 27%, Cu_2O loosed interest as an absorbing material. Instead, its p-type nature made this oxide interesting as a hole transporting layer (HTL) since the currently used material in planar perovskite solar cells, the SpiroMeOTAD, suffers from high cost and limited long-term stability. Beyond its favorable electrical properties, Cu_2O represents a promising HTL alternative due to its suitable energy-level alignment with a wide range of perovskite materials.[6–8] The intrinsic, p-type Cu_2O conductivity is generally attributed to the presence of copper vacancies, which show an acceptor character and easily form thanks to their low formation energy.[9–11] Recent theoretical calculations have shown that copper vacancies may form in a normal configuration, V_{Cu}, and a split configuration, $V_{Cu,split}$, with similar formation energies. These two vacancies induce electronic energy levels located at ~0.2 eV and 0.4–0.5 eV from the valence band maximum (VBM), respectively.[10,12] In particular, values of 0.22 eV and 0.47 eV above VBM have been reported by Scanlon *et al.* for V_{Cu} and $V_{Cu,split}$,[12] in a close agreement with measured values of 0.2 eV and 0.5 eV reported by Paul *et al.*,[8] and 0.22 eV and ~0.4 eV reported by Nyborg *et al.*,[10] respectively. These results indicate a weak shallow and a deep acceptor character for the two vacancy configurations, respectively, which explain why the native p-type doping leads to low hole concentrations in Cu_2O films. This moderate p-type character implies that the pristine Cu_2O resistivity is too high for its exploitation in optoelectronic devices, *e.g.*, most reported resistivity values are higher than 1 Ω cm. Lower resistivity values are mainly obtained by nitrogen doping, which is the most undertaken route for a resistivity lowering.[13–20] Nitrogen could be introduced in the Cu_2O lattice as an oxygen substitute, N_O, or in the molecular form when an N_2 molecule occupies a V_{Cu} site, $(N_2)_{Cu}$. Recent theoretical calculations indicate N_O as a deep

[a] CNR, Istituto di Struttura della Materia, Via del Fosso del Cavaliere 100, 00133 Roma, Italy. E-mail: antonio.ditrolio@cnr.it
[b] CHOSE – Dept. Electronic Engineering University of Rome Tor Vergata, via del Politecnico 1, 00133 Rome, Italy
[c] CNR, Istituto di Struttura della Materia, Via Salaria km 29,300, Montelibretti (RM), Italy

acceptor (inducing an energy level at 0.5 eV above VBM) and $(N_2)_{Cu}$ as a shallow acceptor (inducing a level at about 0.2 eV above VBM).[21] These results fully agree with those of electron energy loss spectroscopy measurements which show the presence of nitrogen in the molecular form and rule out that of N_O in Cu_2O thin films showing improved electron mobility and resistivity values.[22] Cu_2O nitrogen doping was also investigated by performing nitrogen ion implantation.[23] In that study, a shift of the Fermi level towards the valence band maximum was observed, thus fully confirming the nitrogen acceptor behavior. To the best of our knowledge, low resistivity values (<1 Ω cm) in nitrogen doped Cu_2O were obtained by Wang *et al.*,[22] (0.8 Ω cm) in film grown at room temperature, and by Rezek *et al.* (0.05 Ω cm) in films grown at 190 °C.[17] A resistivity value of 0.4 Ω cm was also obtained for Cu_2O films grown at 260 °C by atomic layer deposition with N_2 as the carrier gas by Sekkat *et al.*[18] Cu_2O hydrogen doping was also reported.[10,24–28] In this regard, first studies investigated the effects induced by post-growth hydrogenation treatments on the properties of Cu_2O and N doped Cu_2O polycrystalline films.[25,26,28] These studies reported a decrease of the hole density and an increase of Hall mobility and resistivity in hydrogenated Cu_2O, possibly induced by a H passivation of oxygen dangling bonds (O-DB's) present in acceptor defects (as in the case of the V_{Cu}'s). Instead, in the case of hydrogenated N doped films, an increase of the hole density and a decrease of Hall mobility and resistivity were explained by proposing a H passivation of donor defects possibly involving Cu-DB's. A subsequent, theoretical study accounted for those experimental findings by showing that interstitial H in Cu_2O behaves as a deep amphoteric impurity able to compensate both shallow acceptors and donors.[29] Moreover, regarding the H interaction with acceptor defects, the same study showed that hydrogen can form H-V_{Cu} complexes with low formation energy where the H atoms bind to O-DB's.[29] These complexes induce an ultra-deep acceptor level at about 1.2 eV above the VBM, thus neutralizing the V_{Cu} acceptor effect (this result was supported by a subsequent experimental study on defects in single crystal Cu_2O[10]). A similar hydrogen effect is expected in the case of O-DB's belonging to acceptor defects which may occur at the grain boundaries in polycrystalline Cu_2O. The investigation of H interaction with shallow donors is instead somewhat lacking. The same theoretical study showed that, despite the presence of Cu-DB's in the oxygen vacancy, V_O, this defect does not behave as a donor. Moreover, a H atom interacts with a V_O by occupying the O site and forming an amphoteric H_O defect. No indications were given instead on a possible passivation of Cu-DB's and related donor defects occurring inside, or at the boundaries of, the grains of Cu_2O films. Such a lack of information was somewhat compensated by a subsequent study, where, differently from the above-mentioned studies, hydrogen was introduced during the RF sputtering growth of undoped Cu_2O films.[24] As a further peculiarity of this study, the growth process was performed at high temperatures. This induced an increase of the grain size and a H accumulation at the grain boundaries of the polycrystalline films. The same study reported an increase of Hall mobility and a decrease of resistivity together with a negligible change of the Hall carrier density. These results were explained by showing that H passivated donor defects at the grain boundaries without affecting the acceptor defects present inside the single grains. Finally, in a recent study, the effects of H implantation in undoped Cu_2O films were investigated.[27] This study showed that H can passivate both acceptors and donors. Overall, the above results gave important indications by showing that generally H can compensate/passivate acceptor and donor defects occurring at the boundaries of, or inside, the grains of Cu_2O films, thus affecting the carrier mobility, the carrier densities, and the resistivity values. As a final note, in undoped Cu_2O films deposited in the presence of H_2 gas as well as in films subjected to post-growth H treatments, the achieved resistivity values were higher than 1 Ω cm.[24–26,28] In the present work, it is shown that a remarkable extra-low resistivity of 0.16 Ω cm can be achieved in N and H doped thin Cu_2O films grown by reactive sputtering deposition. Two features distinguish the present approach from the above-mentioned ones: the two dopants are simultaneously introduced in the Cu_2O films during the growth process and the growth is performed at room temperature. The effects of N and H doping on the Cu_2O properties have been investigated by performing resistivity, Hall effect, XRD, UPS (ultraviolet photoelectron spectroscopy), and Raman measurements on four different kinds of samples: pristine Cu_2O, H doped Cu_2O (Cu_2O:H), N doped Cu_2O (Cu_2O:N), and H and N doped Cu_2O (Cu_2O:N/H). Such a systematic investigation of the effects induced by each dopant has permitted to perform a comparative analysis of the achieved results and data from literature and to draw a consistent, interpretative picture explaining the role of the native defects as well as of the N and H dopants in the resistivity reduction.

2. Experimental

Pure, H doped, N doped, and H and N doped Cu_2O thin films, with thickness of 50 nm, were deposited by reactive radio-frequency (RF) magnetron sputtering, employing a Meivac MAK multisource equipped with $3 \times 2''$ confocal sputter sources. Prior to each deposition, the chamber was evacuated to a base pressure of 6.2×10^{-6} mbar. The soda lime silica glass substrates of 2.5×2.5 cm^2 were placed at 4 cm from the Cu_2O target (99.99%, purity) and maintained at room temperature throughout the process. During the deposition the working pressure and the RF power were 6×10^{-3} mbar and 25 W, respectively. The N and H doping were realized by adding N_2 or an Ar + H_2 mixture to Ar gas. Field emission scanning electron microscopy ZEISS SIGMA 300 and energy dispersive spectroscopy (EDS) equipped with an Xplore 30 mm^2 EDS detector (Oxford Instruments, UK), were employed to estimate the N content of Cu_2O:N and Cu_2O:N/H thin films using the Oxford Instruments AzTec Software. XRD measurements were conducted using a Panalytical Empyrean diffractometer in

Bragg–Brentano geometry. The system employed a Cu X-ray tube ($K\alpha_1$ = 1.54060 Å, $K\alpha_2$ = 1.54443 Å) as the radiation source and a PixCel 3D detector operating in linear mode for signal detection. The incident beam was conditioned using divergent slits (1/4°–1/2°), and diffraction patterns were recorded over a 2θ range of 5° to 70°. Due to the extremely weak diffracted intensity, each scan required an extended acquisition time of 7 hours. Micro-Raman measurements were performed by a Renishaw inVia spectroscope. 200 acquisitions per point were collected with a 457 nm laser source, setting the laser power at 10% and time exposure at 1 s in order to avoid surface damage. Resistivity, carrier concentration, and mobility were measured by using the four-point probe method as well as a Hall effect measurement system with a 1.1 T electromagnet in the Van der Paw geometry. UPS measurement were performed with angle resolved ultraviolet photoemission spectroscopy (ARUPS). Spectra were recorded in a Vacuum Generators VG-450 ultrahigh-vacuum chamber at a pressure of less than 2.6×10^{-10} mbar. Unpolarized 21.2 eV radiation from a helium discharge lamp was used. The estimated total energy resolution as determined by the analyzer voltages and the width of the He I light was 100 meV, the angular resolution of the hemispherical analyzer was ±1°.

3. Results and discussion

3a. Electrical and optical characterizations

Electrical measurements were preliminarily performed in pure Cu_2O samples and in a set of doped samples obtained varying the concentration of gases in the mixtures. The optimal mixture compositions, which permit to grow Cu_2O films with minimum resistivity, correspond to a 40% of N_2 in the N_2/Ar mixture and a 0.35% of H_2 in the H_2/Ar and H_2/N_2/Ar mixtures. The samples showing minimum resistivity values were selected for all the here performed investigations. The corresponding resistivity, carrier concentration, and mobility values are reported in Table 1. The Hall measurements confirm the p-type character of all of the investigated samples and show a progressive increase of the hole concentration on going from the Cu_2O to the Cu_2O:N/H samples. Such an increase is in agreement with the observed, progressive reduction of the hole mobility, which is generally attributed to scattering on neutral and ionized defect centers.[10]

The N content in the Cu_2O samples were estimated by performing EDS measurements. Table 2 reports the Cu/N atomic ratio measured for four sets of N and N/H doped Cu_2O films grown in the same conditions. These results derive from EDS analyses performed on different micro-areas of each sample. The average Cu/N atomic ratio is about 10 in N- and N/H-doped Cu_2O films. Considering that 1 cm^3 of Cu_2O contains 5.22×10^{22} Cu atoms, such a Cu/N atomic ratio corresponds to a N_2 concentration of 2.6×10^{21} cm^{-3} when nitrogen enters the Cu_2O lattice as N_2. This value well agrees with the results of SIMS measurements of N doped Cu_2O films grown by RF sputtering with a high N content in the process gas.[30]

Table 1 Resistivity, carrier concentration, and mobility of pure and doped Cu_2O samples

Sample	Sheet resistance (Ω/□)	Resistivity (Ω cm)	Carrier concentration (cm^{-3})	Mobility ($cm^2\ V^{-1}\ s^{-1}$)
Cu_2O	$R_{sh} = 1.20 \times 10^6$	$\rho = 6$	5.4×10^{16}	19
Cu_2O:H	$R_{sh} = 1.05 \times 10^6$	$\rho = 3.4$	1.2×10^{17}	15
Cu_2O:N	$R_{sh} = 8.30 \times 10^4$	$\rho = 0.41$	2.7×10^{18}	5.6
Cu_2O:N/H	$R_{sh} = 3.25 \times 10^4$	$\rho = 0.16$	1.2×10^{19}	3.2

Table 2 Cu/N atomic ratios measured by EDS in four different sets of N and N/H doped Cu_2O samples

	Set 1	Set 2	Set 3	Set 4
Cu_2O:N	Cu/N = 10.23	Cu/N = 9.19	Cu/N = 11.5	Cu/N = 9.24
Cu_2O:N/H	Cu/N = 10.33	Cu/N = 9.84	Cu/N = 12.62	Cu/N = 8.12

The optical properties were investigated by measuring the transmittance (T) in UV-Vis-NIR range, between 280 and 1100 nm. In Fig. 1, the transmittance against the photon wavelength, λ, (and the photon energy, E) and the square of the product of absorption coefficient and photon energy against the photon energy, E, are plotted in figures (A) and (B), respectively. The most relevant feature of the T spectra in Fig. 1(A) is the macroscopic difference between the Cu_2O and the Cu_2O:H spectra. This result clearly indicates that hydrogen strongly perturbs the defect electronic levels in the energy gap. In detail, in the Cu_2O spectrum the T values decrease from a maximum occurring for an E value around 2.3 eV towards an almost asymptotic value. The Cu_2O energy gap is estimated equal to 2.55 eV (see below). Thus, there are defect levels absorbing light in the 2.3–2.5 eV E range, possibly V_{Cu} vacancies that induce acceptor levels about 0.2 eV above VBM. For decreasing E values, the observed T lowering is induced by deep defects levels involved in the light absorption. Differently from Cu_2O, the Cu_2O:H spectrum does not show a maximum T value. A steep T rise in the 3.5–2.5 eV E range is followed by a monotonic T increase for decreasing E values. These results show that both the V_{Cu} acceptor levels and the deep defect levels occurring in the Cu_2O energy gap have been neutralized by the hydrogen introduction. This agrees with the above-mentioned results indicating that H behaves as an amphoteric impurity able to compensate/neutralize both acceptors and donors. Finally, they should be noted the similarities between the Cu_2O and Cu_2O:N spectra on one side and between the Cu_2O:H and Cu_2O:N/H spectra on the other side, which further confirm the relevant role of hydrogen on the transmittance evolution in the here investigated samples.

In Fig. 1(B), the optical band gap (E_g) of the Cu_2O thin films was estimated based on the Tauc relation for allowed direct transitions $(\alpha h\nu)^2 = A(h\nu - E_g)$ where A is a constant, $h\nu$ is the photon energy, E_g is the allowed energy gap, and the absorption coefficient (α) is calculated from $\alpha = -(\log T)/d$, where d is the film thickness. The values for the optical band gaps, estimated by extrapolating the linear portion of the Tauc plots to the energy axis intercept, are 2.52 eV for Cu_2O:N and Cu_2O:N/H, 2.55 eV for Cu_2O, and 2.60 eV for the Cu_2O:H sample. Such

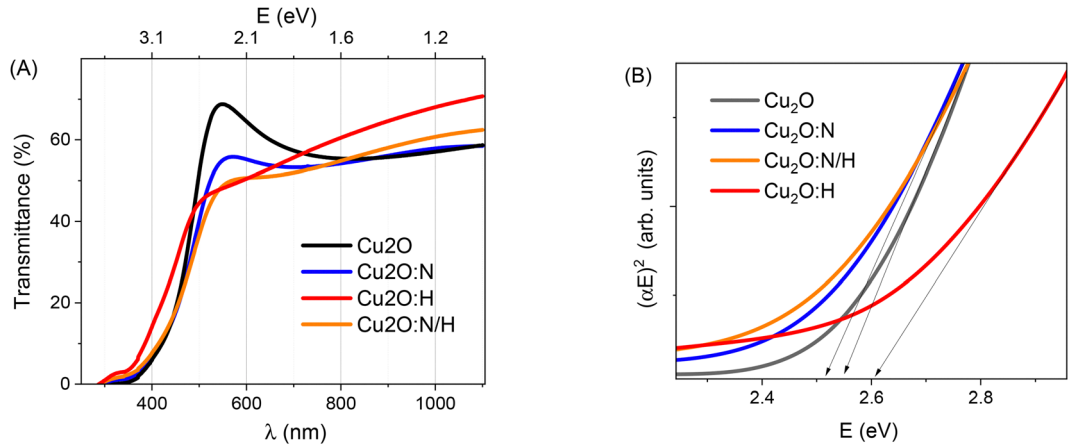

Fig. 1 (A) UV-vis-NIR transmittance spectra against the photon wavelength, λ (and the photon energy, E), and (B) Tauc plot against the photon energy, E, of pure and doped Cu_2O films. The arrows indicate the estimated optical band gaps (the band gap values are basically identical for the Cu_2O:N and Cu_2O:N/H samples).

values are consistent with many reported results[31–33] and with the above discussed H effects.

3b. Structural characterization

XRD spectra were collected to exclude the presence of secondary phases possibly forming during the growth, since Cu_2O is not the thermodynamically most stable phase in the Cu–O binary phase diagram. The experimental diffraction patterns are reported in Fig. 2, while a comparative analysis is summarized in Table 3. Error bars are omitted in the table for clarity and are discussed in the main text. All of the films deposited in Ar, Ar + H_2, Ar + N_2, and Ar + N_2 + H_2 atmospheres exhibit the cubic Cu_2O phase (ICSD Card No. 031057) as the dominant crystalline component, identified by the characteristic (111) and (020) reflections. In all samples, the most intense peak corresponds to the Cu_2O (111) reflection (relative intensity of 100%). For films deposited in Ar (Cu_2O), Ar + H_2 (Cu_2O:H), and Ar + N_2 (Cu_2O:N), the (111) peak is located at 36.41°, while a slight shift to a lower angle (36.29°) is observed for the film grown in Ar + N_2 + H_2 (Cu_2O:N/H), corresponding to a relative variation of ~0.3%. This shift suggests a small increase of the interplanar spacing from 2.469 ± 0.001 Å to 2.471 ± 0.001 Å, corresponding to a relative lattice distortion of ~0.08% along the ⟨111⟩ direction and to a derived lattice parameter variation from 4.272 ± 0.001 Å to 4.281 ± 0.002 Å. A similar, but weaker, trend is observed for the (020) reflection. The peak position shifts from 42.08° in Cu_2O, corresponding to an interplanar spacing of d(020) = 2.147 ± 0.001 Å, to 41.99° and 41.97° in Cu_2O:N/H and Cu_2O:N, corresponding to d(020) = 2.151 ± 0.001 Å and 2.152 ± 0.001 Å, respectively. These shifts correspond to a relative increase in the d-spacing of approximately 0.2%, indicating minor lattice distortions in samples Cu_2O:N/H and Cu_2O:N. A more pronounced shift is observed for the secondary (020) reflection in the Cu_2O:H sample. In this case, the peak position changes from 42.08° in the Cu_2O reference sample, corresponding to an interplanar spacing of d(020) = 2.147 ± 0.001 Å and to a derived lattice parameter a = 4.294 ± 0.002 Å, to 41.28° in Cu_2O:H sample, corresponding to d(020) = 2.188 ± 0.001 Å and to a derived lattice parameter a = 4.376 ± 0.002 Å. Such an appreciable angular shift of 0.80° corresponds to an increase in the interplanar spacing of $\Delta d \approx 0.041$ Å, corresponding to a relative variation of approximately 1.9%, and to a corresponding lattice parameter expansion along the (020) direction. Such a significant and anisotropic lattice expansion likely indicates a structural modification induced by hydrogen incorporation in the Cu_2O:H film. In addition to the peak position shift, the Cu_2O:H sample exhibits the lowest relative intensity of the (020) reflection within the series: the (020) peak reaches only 19% of the (111) intensity, compared to 42%, 49%, and 73% for samples Cu_2O, Cu_2O:N, and Cu_2O:N/H, respectively. This strong suppression of the (020) intensity can be interpreted as a combined effect of preferred orientation and microstructural factors. Cu_2O thin-film studies have shown that changes in deposition conditions and post-treatments can significantly modify grain

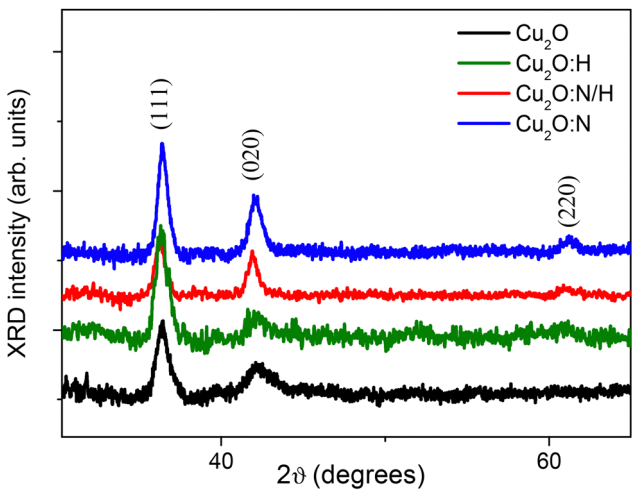

Fig. 2 XRD Diffractograms of Cu_2O films. Miller indexes correspond to the cubic Cu_2O phase.

Table 3 Comparative XRD analysis of pure and doped Cu_2O samples

Peak Position (°)	Index(s)	Element	Intensity	Relative Intensity (%)	System	FWHM (°)	Crystallite Size (nm)	Card no.	Ref.
Sample ID	Cu_2O								
36.41	(111)	Cu_2O	1275	100	Cubic	0.76	11.6	031057	ICSD CC
42.08	(020)	Cu_2O	534	42	Cubic	1.05	8.3	031057	ICSD CC
Sample ID	Cu_2O:N/H								
36.29	(111)	Cu_2O	1580	100	Cubic	0.56	15.6	031057	ICSD CC
41.99	(020)	Cu_2O	1159	73	Cubic	0.54	16.5	031057	ICSD CC
Sample ID	Cu_2O:N								
36.41	(111)	Cu_2O	3762	100	Cubic	0.61	14.2	031057	ICSD CC
41.97	(020)	Cu_2O	1849	49	Cubic	0.77	11.6	031057	ICSD CC
Sample ID	Cu_2O:H								
36.40	(111)	Cu_2O	1486	100	Cubic	0.76	11.0	031057	ICSD CC
41.28	(020)	Cu_2O	279	19	Cubic	1.19	7.4	031057	ICSD CC

morphology and texture, leading to systematic variations in the $I(111)/I(200)$ (or $I(111)/I(020)$) ratio, which correlate with grain size, strain, and defect distribution in different crystallographic directions.[34,35] In sample Cu_2O:H, the (020) reflection not only shifts but also displays the largest FWHM (1.19°) and the smallest crystallite size (7.4 nm) among the examined films, indicating a reduced coherent scattering domain and enhanced microstrain along this orientation. Such a microstructural disorder induces peak broadening and intensity attenuation, providing a possible explanation for the low (020) relative intensity compared to the stronger (111) reflection. Nevertheless, the diffraction pattern of sample Cu_2O:H remains fully consistent with a single cubic Cu_2O phase, and no additional reflections attributable to CuO or metallic Cu are detected. Regarding the crystallite size, sample Cu_2O:N/H possesses the largest crystallites, samples Cu_2O and Cu_2O:H show the smallest crystallites, while sample Cu_2O:N exhibits an intermediate size. No diffraction signatures corresponding to metallic copper (Cu) or copper oxide (CuO) phases are detected in all of the samples, confirming phase purity. In summary, XRD results indicate that the inclusion of hydrogen in the Cu_2O films induces appreciable structural changes which are substantially mitigated in films deposited in presence of hydrogen and nitrogen.

Micro-Raman measurements exploring the low and the high wavenumber regions (0–1000 cm^{-1} and 2000–2500 cm^{-1} respectively) are reported in Fig. 3. Such spectra show features which provide further information on the lattice quality and defect structure. The substrate was also measured and the so obtained Raman spectra (purple line) is also reported in Fig. 3 to rule out the glass contribution. In perfectly stoichiometric Cu_2O (cuprite), the Raman spectrum is dominated by a single weak first-order F_2g mode near ~109 cm^{-1}. However, when structural disorder or point defects are present, otherwise silent infrared modes become Raman-active, giving rise to characteristic defect-related peaks. In defective Cu_2O, the most frequently observed defect-activated bands are the T_1u modes near ~148 cm^{-1} and ~624–649 cm^{-1}, and the second-order overtone of the silent $2E_u$ mode around ~235 cm^{-1}. These features are widely accepted as fingerprints of the Cu vacancy in the split configuration, $V_{Cu,split}$, whereas the Cu vacancy, V_{Cu}, does not induce appreciable signals.[36] The $V_{Cu,split}$ peak intensity scales with the defect concentration. In all of the present

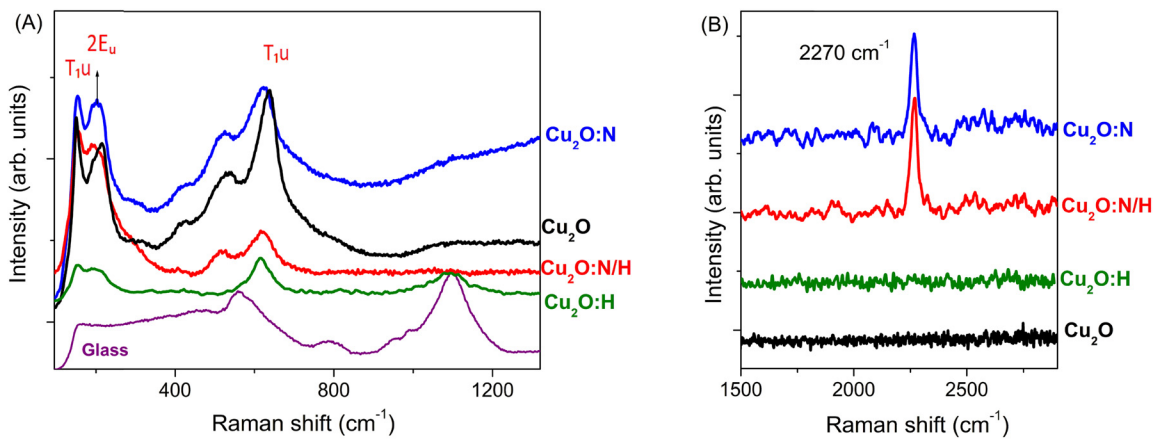

Fig. 3 Micro Raman patterns of Cu_2O films and glass substrate collected in the low (A) and high (B) wavenumber regions.

samples, the spectra display bands at ~153 cm^{-1}, ~210 cm^{-1} and ~620–640 cm^{-1}, as clearly visible in Fig. 3(A). The ~153 cm^{-1} feature is assigned to a defect-activated T_1u mode. This peak maintains its position in all of the present samples. The ~210 cm^{-1} band is attributed to the second-order $2E_u$ overtone. It appears slightly upshifted to ~216 cm^{-1} (closer to the nominal position) in pristine Cu_2O in comparison with the samples Cu_2O:N/H and Cu_2O:H. A smaller shift is observed for the Cu_2O:N sample. A quite similar behavior is shown by the high-frequency line at ~620 cm^{-1}, which corresponds to a T_1u defect-activated mode. Thus, small shifts are observed only in H containing samples. More significant differences are found by comparing the peak intensities of the four sample spectra. First, by assuming Cu_2O as a reference sample, the intensities of all of the three peaks of the Cu_2O:H spectrum are dramatically reduced. This result indicates strong changes of the $V_{Cu,split}$ local configuration induced by the presence of H. Second, still in comparison with Cu_2O, only the intensity of the line at ~620 cm^{-1} is strongly reduced in the Cu_2O:N/H sample. Finally, the intensities of the ~153 cm^{-1} and ~210 cm^{-1} bands show a slight increase in the Cu_2O:N spectrum, which appears, on the whole, very similar to the Cu_2O one. Thus, the presence of H appears to be a key factor to observe a strong or a noticeable perturbation of the $V_{Cu,split}$ configuration.

Finally, as visible in Fig. 3(B), in the high-wavenumber region (2000–2500 cm^{-1}), a distinct band is observed at ~2270 cm^{-1} in samples Cu_2O:N and Cu_2O:N/H, whereas for pristine Cu_2O and Cu_2O:H samples no measurable intensity above the noise level is detected in such region. We attribute the ~2270 cm^{-1} band to the local vibrational mode (LVM) of a defect-bound N_2 dimer, specifically the N_2 substituting on a Cu site $(N_2)_{Cu}$, whose Raman-active stretching mode is expected around ~2280 cm^{-1} after non-harmonic correction (and clearly below the ~2330 cm^{-1} line of free molecular nitrogen). This assignment is consistent with first-principles calculations that predict: (i) $(N_2)_{Cu}$ to be a shallow acceptor, and (ii) an N–N LVM near 2280 cm^{-1} for N_2 on Cu sites, well separated from both the free-molecule value and from the much lower frequencies predicted for N_2 on O sites.[21,22] The absence of any peak near 2330 cm^{-1} in all samples rules out a significant contribution from free or weakly physisorbed N_2, and supports the interpretation that the signal in Cu_2O:N and Cu_2O:N/H originates from N_2 incorporated as a lattice defect rather than from ambient nitrogen.

3c. UPS measurements and electronic structure

UPS spectra of pure and doped Cu_2O, reported in Fig. 4(A), have been measured to explore the relative positions of the Fermi level, E_F, and the valence band maximum, VBM. Such positions have been obtained by linearly extrapolating the leading edge of the spectrum to the baseline. The VBM distance from E_F is 0.5 eV in pure Cu_2O. Then, a shift of the VBM toward the E_F is observed and the E_F-VBM distance decreases progressively to 0.35 eV, 0.25 eV, and 0.15 eV, for the Cu_2O:H, Cu_2O:N, and Cu_2O:N/H samples, respectively. This corresponds to a lowering of the Fermi level towards the VBM, as schematically reported in Fig. 4(B) for each sample. In the figure, the conduction band minimum (CBm) position is set to the mean of the bandgap values estimated from the Tauc plot of Fig. 1(B). A shift of the VBM with respect to the Fermi level was also shown by UPS spectra of N doped Cu_2O obtained by N^+ implantation.[23] In that case, by comparison with pristine Cu_2O, a lowering of the Fermi level of 0.35 eV was observed together with a significant reduction of the electrical resistance. In the present study, the E_F descent toward VBM shown in Fig. 4(B) can be accounted for by the appearance of acceptor states near the VBM. In fact, the results of the Hall measurements show a corresponding, progressive increase of the hole concentrations, see Table 1. The observed E_F evolution is also fully consistent with the results of resistivity measurements. In fact, the resistive value of ρ = 6 Ω cm measured in pristine Cu_2O is in line with the position of E_F at 0.5 eV from VBM. Then, the lowering of ρ to 3.4 Ω cm, 0.41 Ω cm, and 0.16 Ω cm in the samples Cu_2O:H, Cu_2O:N, and Cu_2O:N/H, respectively, is consistent with the

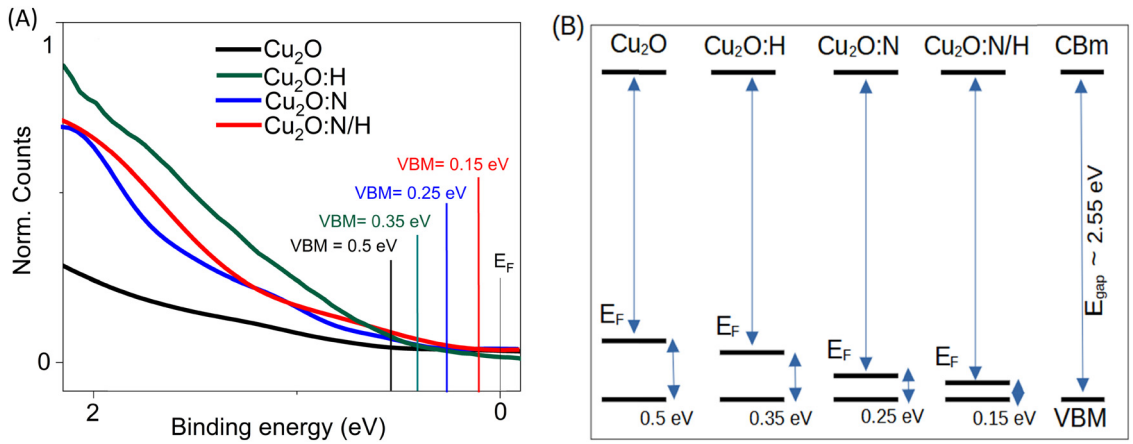

Fig. 4 (A) UPS spectra of pure, H doped, N doped, and N/H-doped Cu_2O thin films. The VBM position is estimated with respect to the Fermi level, E_F. (B) Representative scheme of the Fermi level positions with respect to the VBM. The CBm is set from the bandgap value derived from the Tauc plot of Fig. 1(B).

trend shown by the E_F positions at 0.35 eV, 0.25 eV, and 0.15 eV from VBM, respectively.

3d. Interpretative picture of present results

As illustrated in the previous sections, in the present study, the electrical and structural properties of a pristine Cu_2O sample have been investigated firstly by performing resistivity, Hall effect, XRD, UPS, and Raman measurements. Then, by using this Cu_2O sample as a reference, it has been considered how these same properties are affected by the introduction of H and N, individually, as well as by the simultaneous presence of both dopants. This systematic approach permits to perform a comparative analysis of the achieved results and data from the literature and, then, to draw an interpretative picture explaining the role of native defects and dopants in the evolution of the Cu_2O properties, in particular, in the achievement of a significant resistivity decrease. Such a comparative analysis will be performed here by considering results and data reported in a synoptic Table, see Table 4, to be used as a guide. For the sake of clearness, some of the above-discussed results will be briefly recalled in the following paragraphs.

As a preliminary note, different theoretical studies investigated the properties of native defects in Cu_2O as well as their interaction with H and N dopants. Among them, three recent studies have been selected here, since they use the most accurate, available theoretical methods for the investigation of semiconductor electronic properties and provide results in a good agreement with experimental findings.[12,21,29]

Concerning the pristine Cu_2O properties, one of the mentioned theoretical studies indicates the V_{Cu} and $V_{Cu,split}$ vacancies as the most likely native defects.[12] These two Cu vacancies induce electronic levels in the energy gap 0.23 eV and 0.47 eV above VBM, respectively. These theoretical results are fully supported by experimental findings, see Table 4. Basing on such results, the weak p-type character of the present Cu_2O sample, indicated by a Fermi energy measured at 0.5 eV above VBM, a hole concentration of 5.4×10^{16} cm^{-3}, and a corresponding, moderate resistivity of 6.0 Ω cm can be accounted for by the quasi-shallow electronic level induced by V_{Cu}'s. Regarding the $V_{Cu,split}$ vacancies, the presence of these defects in our sample is proved by the Cu_2O Raman spectrum showing the features generally considered as fingerprints of these defects, see Table 4.

Regarding the effects of H doping on the Cu_2O properties, as discussed in a previous section, a theoretical study[29] supported by the experiments[10] showed that the interaction of atomic H with V_{Cu} leads to the formation of V_{Cu}-H complexes. These complexes are ultra-deep defects inducing an electronic level at ~1.3 eV above VBM, significantly higher than the quasi-shallow and the deep levels induced by V_{Cu} and $V_{Cu,split}$, respectively. Thus, H is expected to fully passivate the acceptor V_{Cu}'s. Here, present results show that in the Cu_2O:H sample a macroscopic change of the Raman spectrum occurs with respect to the Cu_2O spectrum. All of the vibrational line intensities attributed to the $V_{Cu,split}$ vacancies significantly decrease, see Table 4, thus indicating a noticeable change of the local $V_{Cu,split}$ configuration. It should be noted that this $V_{Cu,split}$ evolution parallels the noteworthy lattice variation revealed by the comparison of the Cu_2O and Cu_2O:H XRD results discussed above. Such a major change of the $V_{Cu,split}$ configuration cannot be induced by the scarcely reactive hydrogen molecule. Instead, it can be reasonably assumed that the peculiarities of the here used growth procedure (the Ar atoms and the H_2 molecules undergo an electrical discharge and acquire an increasing kinetic energy before reaching the target) favor the introduction of the more reactive, atomic H in the Cu_2O sample. In presence of H atoms, the formation of V_{Cu}-H complexes and the ensuing V_{Cu} passivation can be safely supposed. On the other hand, although the effects of atomic H interaction with $V_{Cu,split}$ vacancies are unknown, the strong change of the $V_{Cu,split}$ configuration indicated by the Raman results makes highly probable the formation of some kind of V_{Cu}-H complexes, possibly accompanied by a $V_{Cu,split}$ evolution from a deep to an ultra-deep acceptor defect. Anyway, on the whole, the H introduction should induce a reduction of the sample p-type character. Surprisingly, the results achieved for the Cu_2O:H sample show instead an appreciable decrease of the Fermi level distance from VBM, a small decrease of the resistivity value and, most important, an increase of the hole concentration, see Table 4. These unexpected results represent an important indication since they show that H can enhance the Cu_2O p-type character despite its ability to passivate the acceptor V_{Cu}'s initially responsible of such a character. These results are further surprising because the above-mentioned theoretical study[29] excludes the appearance of new, shallow acceptor defects induced by some H effect. Moreover, the same study and the results of the experimental studies discussed

Table 4 Synoptic table reporting present values of resistivity, ρ, Fermi energy position with respect to the valence band maximum (VBM), E_F, hole concentrations, experimental and theoretical estimates of the positions of defect electronic levels with respect to VBM taken from the literature, positions of Raman lines in spectra measured in the present work (p.w.) and taken from literature (liter.). In the table, the arrows ↓ indicate a significant decrease of the Raman line intensity

Sample	ρ (Ω cm)	E_F (eV)	Hole conc. (cm^{-3})	Electr. lev. eV (exp)[10]	Electr. lev. eV (theor.)[12,21,29]	Raman cm^{-1} (p.w.)	Raman cm^{-1} (liter.)
Cu_2O	6.00	0.50	5.4×10^{16}	0.22 (V_{Cu}), ~0.4 (V_{Cu}-s)	0.23 (V_{Cu}), 0.47 (V_{Cu}-s)[12]	153, 210, 620–640	148, 235, 624–649
Cu_2O:H	5.00	0.35	1.2×10^{17}	~1.3 (V_{Cu}-H)	1.15 (V_{Cu}-H)[29]	153 (↓), 210 (↓), 620–640 (↓)	
Cu_2O:N	0.41	0.25	2.7×10^{18}	0.16 $(N_2)_{Cu}$	0.20 $(N_2)_{Cu}$[21]	153, 210, 620–640, 2270	2280
Cu_2O:N/H	0.16	0.15	1.2×10^{19}	0.16 $(N_2)_{Cu}$, ~1.3 (V_{Cu}-H)	0.20 $(N_2)_{Cu}$[21], 1.15 (V_{Cu}-H)[29]	153, 210, 620–640 (↓), 2270	2280

above[24–28] indicate that H behaves as a deep amphoteric impurity in Cu_2O, able to compensate/neutralize both acceptors and donors. Thus, the only reasonable explanation of the here observed Fermi level descent and hole concentration increase is that H mainly compensates/passivates native donor defects, thus inducing an increase of the acceptor concentration. This result can be related to the findings of the above-mentioned study where H was introduced during the Cu_2O growth and high temperatures favored the occurrence of quite large grains.[24] An increase of the Hall mobility was observed in that study, together with minor changes of the hole concentration. Those results were accounted for by showing that H accumulated at the grain boundaries, where it neutralized donor defects with minor effects on the inner-grain acceptor defects. An investigation of the H effects on the grain boundary defects is beyond the scope of the present work. However, it can be noted that even in the present study H is introduced during the Cu_2O growth, but, the here used room temperature conditions induce the formation of much smaller grains (see Table 3). This results in a higher, overall surface/volume ratio. Thus, it can be suggested that, similarly to the mentioned study, H accumulated at the grain boundaries neutralizes donor defects to a greater extent than inner-grain acceptors and this effect is amplified by the larger exposed surface, thus accounting for an overall increase of the acceptor number.

About nitrogen doping, a recent theoretical study investigated different interstitial and substitutional sites for N atoms and N_2 molecules introduced in the Cu_2O lattice and showed that a N atom substituting an oxygen atom (N_O) and a nitrogen molecule occupying the V_{Cu} site, $(N_2)_{Cu}$, are the lowest energy defects.[21] The latter defect becomes the favorite one in Cu-poor growth conditions. Moreover, N_O and $(N_2)_{Cu}$ behave as a deep and a shallow acceptor, respectively. These results have been fully confirmed by a subsequent, experimental study which ruled out the formation of N_O and supported that of $(N_2)_{Cu}$ by confirming also the shallow acceptor character of the latter defect,[10] see the position of the corresponding defect electronic levels in Table 4. In the case of the present Cu_2O:N sample, the corresponding Raman spectrum is very similar to the Cu_2O one in the low-wavenumber region (0–1200 cm^{-1} range), see Table 4, thus indicating that N introduced in the sample does not perturb the native $V_{Cu,split}$ vacancies. This indirectly indicates that N is mainly present in the sample in the molecular form, less reactive than the atomic form. The presence of N_2 molecules in our sample should favor the formation of $(N_2)_{Cu}$ complexes. As a matter of fact, such an occurrence is confirmed by the Raman line measured in the Cu_2O:N sample in the high-wavenumber region at 2270 cm^{-1}, close to the value indicated by theory and experiment for the $(N_2)_{Cu}$ complexes.[10,21] Due to their shallow acceptor character, the presence of $(N_2)_{Cu}$ complexes in our sample perfectly accounts for the significant Fermi level descent toward the VBM, the significant increase of the hole concentration, as well as for the consistent, remarkable resistivity decrease, observed in the Cu_2O:N sample in comparison with the Cu_2O one, see Table 4.

Finally, a further Fermi level descent toward VBM and a parallel increase of the hole concentration and resistivity decrease characterize the simultaneous doping with N and H realized in the Cu_2O:N/H sample in comparison with the Cu_2O:N one. In the former sample, driven by the above results, we expect that N_2 molecules occupy the V_{Cu} sites by forming $(N_2)_{Cu}$ shallow acceptors. Moreover, by considering that the formation of V_{Cu}-H complexes comes from the H interaction with the O dangling bonds facing the V_{Cu} site and that, in the $(N_2)_{Cu}$ complex, these dangling bonds are not available (since involved in the formation of O–N bonds), we expect that such a complex is not affected by the presence of H atoms. Actually, the occurrence of unperturbed $(N_2)_{Cu}$ complexes in our sample is confirmed by the appearance of the above-mentioned line at 2270 cm^{-1} also in the Cu_2O:N/H Raman spectrum. As discussed above, instead, atomic H can strongly perturb the $V_{Cu,split}$ vacancies. These vacancies are not affected by the presence of N_2 molecules, as shown by the similarity of the low-wavenumber region Cu_2O:N Raman spectrum with that of the pristine Cu_2O, see Table 4. Thus, in principle, even in the Cu_2O:N/H film, H should induce strong changes of the $V_{Cu,split}$ configuration as those indicated by the evolution of the Cu_2O:H Raman spectrum, see Table 4. In a partial agreement with such an expectation, in comparison with the Cu_2O and Cu_2O:H Raman spectra, in the low-wavenumber region the Cu_2O:N/H Raman spectrum shows a significant reduction of the peak intensity only in the case of the 620–640 cm^{-1} line. This suggests the occurrence of an appreciable change of the local $V_{Cu,split}$ configuration induced by the interaction with H which seems to be, however, somewhat different from that occurring in the Cu_2O:H sample. It should be noted, once again, that the occurrence of a $V_{Cu,split}$ configuration change in the Cu_2O:N/H sample agrees with the small, but still appreciable, lattice variation observed in this sample with respect to pristine Cu_2O, discussed above. Basing on all of the above results and considerations, in the case of the simultaneous N and H doping of Cu_2O, we can draw the following conclusions: (i) N_2 molecules introduced in the Cu_2O lattice occupy the V_{Cu} sites by forming $(N_2)_{Cu}$ shallow acceptors, (ii) hydrogen introduced in the atomic form during the growth procedure does not perturb the $(N_2)_{Cu}$ complexes, (iii) H atoms induce some configuration change of the $V_{Cu,split}$ vacancies (which are not affected by the presence of N_2 molecules), and (iv) as discussed above, hydrogen mainly compensates/neutralizes native shallow donors, thus making active the $(N_2)_{Cu}$ acceptors that are compensated in the Cu_2O:N sample. This leads to an overall increase of shallow acceptors, thus accounting well for the further Fermi level descent, hole concentration increase, and resistivity decrease observed in the Cu_2O:N/H sample with respect to the Cu_2O:N one.

In conclusion, the above analysis shows that all of the present results can be collected in a coherent, qualitative picture which fully accounts for how an extra-low resistivity can be achieved in nitrogen and hydrogen doped Cu_2O films.

4. Conclusions

In the present study, it is shown that Cu_2O films with an extra-low resistivity can be grown by RF sputtering by exploiting nitrogen and hydrogen doping. Significantly, two peculiar features distinguish the present study from previous ones: the two dopants are simultaneously introduced in the Cu_2O films during the growth and the growth process is performed at room temperature. The effects of N and H doping on the Cu_2O properties have been investigated by performing resistivity, Hall effect, XRD, UPS and Raman measurements on four different kinds of samples: a pristine Cu_2O film, Cu_2O films doped with N and H individually, as well as a Cu_2O film containing both dopants. Such a systematic investigation of the doping effects has permitted to perform a comparative analysis of the achieved results and data from literature and to draw a sound, consistent picture explaining the role of native defects and the N and H dopants in the successful achievement of extra-low resistivity values.

Author contributions

ADT, ADC and AAB conceived the idea and planned the work. Film growth, PML, SA and ADT; XRD and Raman characterization, BP, AG; transmittance measurements, PML, SA; UPS characterization, AC, DB, and ML; writing – original draft preparation, ADT and AAB; and writing – review and editing, ADC, ADT, BP, AAB, FF. All authors discussed the results and commented on the manuscript.

Conflicts of interest

There are no conflicts to declare.

Data availability

The data supporting this study are available in the published article and at https://Zenodo.org, DOI:https://doi.org/10.5281/zenodo.18771428.

Acknowledgements

The research was funded by the national project *Ricerca di Sistema Elettrico* of the Ministero dell'Ambiente e della Sicurezza Energetica (RdS25-27). The authors are grateful to Mr Marco Guaragno and Mr Luca Imperatori (ISM CNR) for the technical support with the XRD and EDS measurements.

References

1 S. Chen, L. Wang, C. Zhou and J. Yang, A review of Cu_2O solar cell, *J. Renewable Sustainable Energy*, 2023, **15**, 062701.
2 S. Chen, L. Wang, C. Zhou, J. Yang and X. Jia, Simulation Analysis of Cu_2O Solar Cells, *Energies*, 2025, **18**, 5623.
3 S. Yoshio, A. Wada, S. Shibasaki, N. Nakagawa, Y. Mizuno, Y. Honishi, K. Wakamatsu, M. Toyota, T. Yamamoto, J. Sano *et al.*, Thermal stability of cuprous oxide top cells for high-efficiency Cu_2O/Si tandem solar cells, *in Proceedings of the 2024 IEEE, 52nd Photovoltaic Specialist Conference (PVSC)*, Seattle, WA, USA, 9–14 June 2024; pp. 0149–0151.
4 Toshiba, see https://www.global.toshiba/ww/technology/corporate/rdc/rd/topics/22/2209-02.html for "Toshiba boosts transparent Cu_2O tandem solar cell to a new high".
5 S. Ruhle, Tabulated values of the Shockley-Queisser limit for single junction solar cells, *Sol. Energy*, 2016, **130**, 139.
6 S. Chatterjee and A. J. Pal, Introducing Cu_2O Thin Films as a Hole-Transport Layer in Efficient Planar Perovskite Solar Cell Structures, *J. Phys. Chem. C*, 2016, **120**, 1428.
7 Y. Guo, H. Lei, L. Xiong, B. Li, Z. Chen, J. Wen, G. Yang, G. Li and G. Fang, Single phase, high hole mobility Cu_2O films as an efficient and robust hole transporting layer for organic solar cells, *J. Mater. Chem. A*, 2017, **5**, 11055.
8 Y. Wang, A. Steigert, G. Yin, V. Parvan, R. Klenk, R. Schlatmann and I. Lauermann, Cu_2O as a Potential Intermediate Transparent Conducting Oxide Layer for Monolithic Perovskite-CIGSe Tandem Solar Cells, *Phys. Status Solidi C*, 2017, **14**, 1700164.
9 G. K. Paul, Y. Nawa, H. Sato, T. Sakurai and K. Akimoto, Defects in studied by deep level transient Spectroscopy, *Appl. Phys. Lett.*, 2006, **88**, 141901.
10 M. Nyborg, I. Kolevatov, G. C. Vàsquez and K. Bergum, Dominant defects and carrier transport in single crystalline cuprous oxide: A new attribution of optical transitions, *J. Appl. Phys.*, 2021, **130**, 175701.
11 A. F. Wright and J. S. Nelson, Theory of the copper vacancy in cuprous oxide, *J. Appl. Phys.*, 2002, **92**, 5849.
12 D. O. Scanlon, B. J. Morgan and G. W. Watson, Acceptor Levels in p-Type Cu_2O: Rationalizing Theory and Experimen, *Phys. Rev. Lett.*, 2009, **103**, 096405.
13 S. Ishizuka, S. Kato, Y. Okamoto, T. Maruyama and K. Akimoto, Nitrogen doping into Cu_2O thin films deposited by Reactive Radio-Frequency Magnetron Sputtering, *Jpn. J. Appl. Phys.*, 2001, **40**, 2765.
14 C. Malerba, C. L. Azanza Ricardo, M. D'Incau, F. Biccari, P. Scardi and A. Mittiga, Nitrogen doped Cu_2O: A possible material for intermediate band solar cells, *Sol. Energy Mater. Sol. Cells*, 2012, **105**, 192.
15 J. Benz, K. P. Hering, B. Kramm, A. Polity, P. J. Klar, S. C. Siah and T. Buonassisi, The influence of nitrogen doping on the electrical and vibrational properties of Cu_2O, *Phys. Status Solidi B*, 2017, **254**, 1600421.
16 J. Li, Z. Mei, L. Liu, H. Liang, A. Azarov, A. Kuznetsov, Y. Liu, A. Ji, Q. Meng and X. Du, Probing Defects in Nitrogen-Doped Cu_2O, *Sci. Rep.*, 2014, **4**, 7240.
17 J. Rezek, J. Koloros, J. Houska, R. Cerstvý, S. Haviar, D. Kolenatý, J. Y. Damte and P. Baroch, Ultra-low-resistivity nitrogen-doped p-type Cu_2O thin films fabricated by reactive HiPIMS, *Appl. Surf. Sci.*, 2025, **714**, 164380.
18 A. Sekkat, M. O. Liedke, V. H. Nguyen, M. Butterling, F. Baiutti, J. de Dios Sirvent Veru, M. Weber, L. Rapenne, D. Bellet,

G. Chichignoud, A. Kaminski-Cachopo, E. Hirschmann, A. Wagner and D. Muñoz-Rojas, Chemical deposition of Cu_2O films with ultra-low resistivity: correlation with the defect landscape, *Nat. Commun.*, 2022, **13**, 5322.

19 A. Sekkat, V. H. Nguyen, C. A. Masse de la Huerta, L. Rapenne, D. Bellet, A. Kaminski-Cachopo, G. Chichignoud and D. Muñoz-Rojas, Open-air printing of Cu_2O thin films with high hole mobility for semitransparent solar harvesters, *Commun. Mater.*, 2021, **2**, 78.

20 P. Mijangos-Alonzo, O. Vigil-Galán, M. Acosta, R. Hernández Castillo, M. M. Nicolás-Marín and I. Riech, Room temperature RF-sputtered Cu_2O thin films: a promising hole transport layer for antimony chalcogenide solar cells, *Semicond. Sci. Technol.*, 2025, **40**, 045002.

21 J. T-Thienprasert and S. Limpijumnong, Identification of nitrogen acceptor in Cu_2O: First-principles Study, *Appl. Phys. Lett.*, 2015, **107**, 221905.

22 Y. Wang, J. Ghanbaja, D. Horwat, L. Yu and J. F. Pierson, Nitrogen chemical state in N-doped Cu_2O thin films, *Appl. Phys. Lett.*, 2017, **110**, 131902.

23 M. Jorge, S. M. Polyakov, S. Cooil, A. K. Schenk, M. Edmonds, L. Thomsen, F. Mazzola and J. W. Wells, Robust p-type doping of copper oxide using nitrogen implantation, *Mater. Res. Express*, 2017, **4**, 075905.

24 K. P. Hering, C. Kandzia, J. Benz, B. G. Kramm, M. Eickhoff and P. J. Klar, Hydrogen induced mobility enhancement in RF sputtered Cu_2O thin films, *J. Appl. Phys.*, 2016, **120**, 185705.

25 S. Ishizuka, S. Kato, Y. Okamoto and K. Akimoto, Hydrogen treatment for polycrystalline nitrogen-doped Cu_2O thin film, *J. Cryst. Growth*, 2002, **616**, 237.

26 S. Ishizuka, S. Kato, Y. Okamoto, T. Sakurai, K. Akimoto, N. Fujiwara and H. Kobayashi, Passivation of defects in polycrystalline Cu_2O thin films by hydrogen or cyanide treatment, *Appl. Surf. Sci.*, 2003, **216**, 94.

27 R. Kumar, K. Bergum, H. N. Riise, E. Monakhov, A. Galeckas and B. G. Svensson, Impact of post annealing and hydrogen implantation on functional properties of Cu_2O thin films for photovoltaic applications, *J. Alloys Compd.*, 2020, **825**, 153982.

28 Y.-M. Lu, C.-Y. Chen and M. H. Lin, Effect of hydrogen plasma treatment on the electrical properties of sputtered N-doped cuprous oxide films, *Mater. Sci. Eng. B*, 2005, **118**, 179.

29 D. O. Scanlon and G. W. Watson, Uncovering the Complex Behavior of Hydrogen in Cu_2O, *Phys. Rev. Lett.*, 2011, **106**, 186403.

30 O. Nordseth, R. Kumar, K. Bergum, I. Chilibon, S. E. Foss and E. Monakhov, Nitrogen-Doped Cu_2O Thin Films for Photovoltaic Applications, *Materials*, 2019, **12**, 3038.

31 H. J. Li, C. Y. Pu, C. Y. Ma, S. Li, W. J. Dong, S. Y. Bao and Q. Y. Zhang, Growth behavior and optical properties of N-doped Cu_2O films, *Thin Solid Films*, 2011, **520**, 212.

32 J.-A. Kim, J.-H. Park, S.-G. Park, C.-S. Son, Y.-G. Son and D.-H. Hwang, Effect of Substrate Temperature on Variations in the Structural and Optical Properties of Cu_2O Thin Films Deposited via RF Magnetron sputtering, *Crystals*, 2023, **13**, 643.

33 D. Chua, S. Bok Kim, K. Li and R. Gordon, Low Temperature Chemical Vapor Deposition of Cuprous Oxide Thin Films Using a Copper(I) Amidinate Precursor, *ACS Appl. Energy Mater.*, 2019, **2**, 7750.

34 Z. Q. Yao, S. L. Liu, L. Zhang, B. He, A. Kumar, X. Jiang, W. J. Zhang and G. Shao, Room temperature fabrication of p-channel Cu_2O thin-film transistors on flexible polyethylene terephthalate substrates, *Appl. Phys. Lett.*, 2012, **101**, 042114.

35 A. Paracchino, J. C. Brauer, J.-E. Moser, E. Thimsen and M. Graetzel, Synthesis and Characterization of High-Photoactivity Electrodeposited Cu_2O Solar Absorber by Photoelectrochemistry and Ultrafast Spectroscopy, *J. Phys. Chem. C*, 2012, **116**, 7341.

36 T. Sander, C. T. Reindl, M. Giar, B. Eifert, M. Heinemann, C. Heiliger and P. J. Klar, Correlation of intrinsic point defects and the Raman modes of cuprous oxide, *Phys. Rev. B: Condens. Matter Mater. Phys.*, 2014, **90**, 045203.